Radiation by Cavity-backed Antennas on a Circular Cylinder

Leo C. Kempel, John L. Volakis and Randy Sliva
Radiation Laboratory
University of Michigan
1301 Beal Ave.
Ann Arbor, MI 48109-2122

December 10, 1993

Abstract

Conformal antenna arrays are popular antennas for aircraft, spacecraft and land vehicle platforms due to their inherent low weight, cost and drag properties. However, to date there has been a dearth of rigorous analytical or numerical solutions to aid the designer. In fact, it has been common practice to use limited measurements and planar approximations in designing such non-planar antennas. In this paper, we extend the finite element-boundary integral method to radiation by cavity-backed structures in an infinite, metallic cylinder. The formulation is used to investigate the effect of cavity size on the radiation pattern for typical circumferentially and axially polarized patch antennas. Curvature effect on the gain, pattern shape and input impedance is also studied. Finally, the accuracy of the FE-BI approach for a microstrip patch array is demonstrated.

1 Introduction

Modern aircraft and missile deigns seek to utilize conformal antenna arrays rather than conventional protruding antennas due to their low weight, low drag, low cost and flexibility. Although most useful aircraft surfaces possess some curvature, the vast majority of available design information is restricted to planar elements. Indeed, the literature is rich with approximate [1], numerical [2] and experimental [3] design and characterization data for planar structures. The most common antenna element is a microstrip patch printed on a dielectric coated groundplane. Dielectric coated cylinders have also been investigated using approximate [4] and numerical [5] approaches.

Often, it is desirable to enclose each radiating element within a metallic cavity to suppress parasitic substrate coupling [6]. Approximate models, such as the cavity model, are typically not modified to account for the metallic sidewalls of the surrounding cavity since the approximations involved in this approach limits its operation to resonant patches. Experience has shown that a surrounding cavity does not effect the radiation pattern of a resonant patch antenna. However, since integral equation formulations are meant to operate at any frequency, these formulations need be modified to account for the metallic sidewalls. This is done by partitioning the problem into an interior cavity region and an open exterior region and enforcing field continuity across the aperture. Such an approach requires a complicated dyadic Green's function for the interior region and as is the case with all integral equation formulations, the resulting linear system is associated with a fully populated matrix and hence imposes a large $\mathcal{O}(N^2)$ memory and computation demand. Additionally, most integral equation formulations utilize equivalent surface currents and are therefore inappropriate for modeling inhomogeneous substrates.

An alternative formulation, utilizing the Finite Element-Boundary Integral (FE-BI) method, was proposed by Jin and Volakis [7] which was suitable for cavity-backed antennas recessed in a metallic groundplane. As with all partial differential equation formulations, this approach is associated with a highly sparse system which requires only $\mathcal{O}(N)$ storage. Additionally, when coupled with a Biconjugate Gradient-Fast Fourier Transform (BiCG-FFT) solver, the computational burden is only $\mathcal{O}(N\log(N))$. Since this approach is a volume formulation, inhomogeneous substrates may be readily modeled. This FE-BI method has been successfully used for scattering and antenna

performance analysis in planar platforms.

Recently, the FE-BI method was extended to cylindrical-rectangular and wraparound cavities for scattering calculations [8]. New divergence free, high fidelity edge-based elements were presented along with an efficient solution strategy which exploited an asymptotic evaluation of the appropriate dyadic Green's function as well as the BiCG-FFT solver. The resulting computer code was shown to accurately compute the scattering by planar and highly curved elements. This paper investigates the accuracy of this FE-BI method formulation for antenna performance analysis. Both radiation pattern and input impedance calculations will be compared with known results. The effect of curvature on the pattern shape, the resonance behavior and the input impedance will be explored.

2 Formulation

In this section, the FE-BI formulation appropriate for radiation analysis is developed for cavity-backed antennas recessed in an infinite metallic cylinder (see figure 1). As usual, the finite element formulation permits substantial modeling flexibility, including cavity inhomogeneities, lumped loads and microstrip feeding lines.

The FE-BI formulation begins with the weak form of the vector wave equation followed by specification of appropriate vector shape functions and dyadic Green's function. The resulting FE-BI equations are then used to solve for the total electric fields within the cavity and on the aperture (see for example Volakis *et al.* [9]). For the specific configuration at hand, the weak form of the wave equation can be written as

$$\int_{V_i} \left\{ \frac{\nabla \times \vec{W}_j(\rho,\phi,z) \cdot \nabla \times \vec{W}_i(\rho,\phi,z)}{\mu_r(\rho,\phi,z)} \right.$$
$$\left. -k_o^2 \epsilon_r(\rho,\phi,z) \vec{W}_j(\rho,\phi,z) \cdot \vec{W}_i(\rho,\phi,z) \right\} \rho \, d\rho \, d\phi \, dz$$
$$+(k_o a)^2 \delta_a(j) \delta_a(i) \int_{S_i} \int_{S_j} \left[\vec{W}_i(a,\phi,z) \cdot \hat{\rho}(a,\phi,z) \times \right.$$
$$\left. \overline{\overline{G}}_2(a,\bar{\phi},\bar{z}) \times \hat{\rho}(a,\phi',z') \cdot \vec{W}_j(a,\phi',z') \right] d\phi' \, dz' d\phi \, dz = f_i^{int} + f_i^{ext} \quad (1)$$

In this, $\vec{W}_i$ are vector basis functions with support over the volume V_i which is

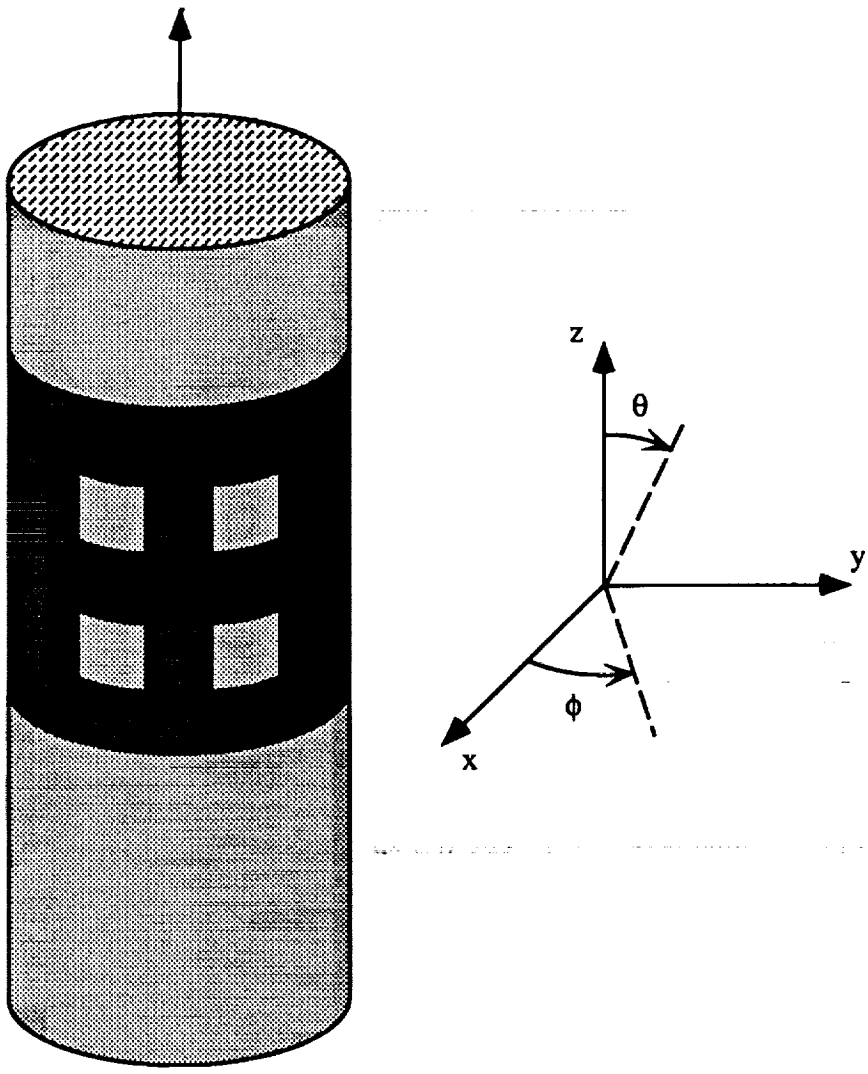

Figure 1: Illustration of a typical cavity-backed antenna situated on a metallic cylinder and the associated coordinate system.

associated with the i^{th} degree of freedom, and in a similar fashion, S_i and S_j represent aperture surfaces associated with the i^{th} and j^{th} degrees of freedom, respectively. The appropriate dyadic Green's function is denoted by $\overline{\overline{G}}_2$ and it has convolutional ($\bar{\phi} = \phi - \phi'$, $\bar{z} = z - z'$) form when evaluated on the surface of the cylinder, $\rho = a$. The unprimed coordinates represent the test point while the primed ones denote the source point. The free-space propagation constant is given by $k_0 = \frac{2\pi}{\lambda_0}$, where λ_0 is the free-space wavelength. The cavity is filled with an inhomogeneous material having relative constitutive properties ϵ_r and μ_r. The function $\delta_a(i)\delta_a(j)$ is the product of two Kronecker delta functions. Hence, it identifies which pairs of unknowns belong to the aperture and accordingly contribute to the boundary integral sub-matrix.

The FEM-BI equation (1) may be rewritten in matrix form as

$$\left[\mathcal{A}\right] \begin{Bmatrix} E_j^{ap} \\ E_j^{int} \end{Bmatrix} + \begin{bmatrix} [\mathcal{G}] & [0] \\ [0] & [0] \end{bmatrix} \begin{Bmatrix} E_j^{ap} \\ E_j^{int} \end{Bmatrix} = \begin{matrix} \{0\} \\ \{f_i^{int}\} \end{matrix} \tag{2}$$

where the entries of $[\mathcal{A}]$ are due to the FEM portion of the formulation and $[\mathcal{G}]$ is the boundary integral sub-matrix. In (2), E_j^{ap} and E_j^{int} denote degrees of freedom associated with the aperture and interior fields, respectively. In this, f_i^{int} are functions of the internal excitation and for this paper a radially oriented probe feed is considered.

The matrix entries, $[\mathcal{A}]$ and $[\mathcal{G}]$, are given in a previous paper [8]. In addition, the vector elements, dyadic Green's function evaluation and far-zone field formulae are given and are therefore not repeated here. Hence, we need only specify the interior source functional in order to model a radiating element. That functional is given for general impressed sources as

$$f_i^{int} = -\int_{V_i} \left\{ \nabla \times \left[\frac{\vec{M}^{int}(\rho,\phi,z)}{\mu_r(\rho,\phi,z)} \right] + jk_o Z_o \vec{J}^{int}(\rho,\phi,z) \right\} \cdot \vec{W}_i(\rho,\phi,z)\rho\, d\rho\, d\phi\, dz \tag{3}$$

where $\vec{J}^{int}$ and $\vec{M}^{int}$ are the impressed electric or magnetic current densities representing the sources. For a radially ($\hat{\rho}$) directed probe feed, the impressed monopole current located at (ϕ_s, z_s) is given by

$$\vec{J}^{int} = \hat{\rho} I_0 \frac{\delta(\phi - \phi_s)(z - z_s)}{\rho} \tag{4}$$

which results in an excitation function (3)

$$f_i^{int} = -jk_oZ_oI_o\frac{\tilde{s}_i\rho_b}{\alpha_i h_i}\ln\left(\frac{\rho_b}{\rho_a}\right)\left[\left(\phi_s-\tilde{\phi}_i\right)\left(z_s-\tilde{z}_i\right)\right] \quad (5)$$

if the edge-based elements of [8] are used.

Having specified the finite element and boundary integral matrices as well as the internal excitation for those systems, we use the BiCG method to solve for the unknown electric fields throughout the computation domain. The FE matrix is highly sparse and hence may be efficiently solved using a sparse matrix-vector product. It is also important to note that the matrix-vector product associated with the boundary integral can be performed using FFTs. Hence, the resulting BiCG-FFT solver is highly efficient without consuming excessive memory resources. The electric field may now be used to compute antenna parameters such as the gain and the input impedance.

The radiation pattern is computed by integrating the aperture fields with the far-zone dyadic Green's function given in [8]

$$\begin{aligned}\vec{H}^r(r,\theta,\phi) &= jY_ok_oa\int_S \overline{\overline{G}}_2(r,\theta,\phi;a,\phi',z')\cdot \\ &\quad \left[\hat{\rho}(a,\phi',z')\times\vec{E}(a,\phi',z')\right]d\phi'\,dz' \end{aligned} \quad (6)$$

with (r,θ,ϕ) indicating the observation point in spherical coordinates. In the far-zone, the electric and magnetic fields are related by

$$\begin{aligned} E_\phi^r &= -Z_oH_\theta^r \\ E_\theta^r &= Z_oH_\phi^r \end{aligned} \quad (7)$$

which is used to compute the antenna gain

$$G_{dB}(\theta,\phi) = 10\log_{10}\left[4\pi\left(\frac{r}{\lambda_{cm}}\right)^2|E^r(\theta,\phi)|^2\right]+10\log_{10}\left[\frac{\lambda_{cm}^2}{Z_oR_{in}}\right] \quad (8)$$

where λ_{cm} is the wavelength in centimeters, R_{in} is the input resistance which is given below and E^r is the radiated electric field as $r\to\infty$.

In addition to the antenna gain, designers are concerned with the input impedance of an antenna for feedline matching purposes. The FEM approach allows the calculation of the input impedance of the radiating structure in a

rather elegant manner. The input impedance is comprised of two contributions [10]

$$Z_{in} = Z_P + Z_D \tag{9}$$

where the first term is the probe's self-impedance (e.g. the probe's impedance in the absence of the patch) and the second term is the contribution of the patch current to the total input impedance. The probe self-impedance accounts for the finite radius of the probe and hence is omitted when a zero-thickness probe is assumed. Ignoring the probe-feed's self impedance, we have [10]

$$Z_{in}^{i} = -\frac{1}{I_o^2}\int_{V_i} \vec{E}(\rho,\phi,z)\cdot\vec{J}_i^{int}(\rho,\phi,z)\rho d\rho d\phi dz \tag{10}$$

where the impressed current is given by (4), V_i refers to the volume elements containing the probe-feed, the electric field is the interior field at (ρ,ϕ,z) and I_o is the constant current impressed on the probe. Utilizing (4) and assuming the edge-based elements presented in [8], the input impedance (10) is evaluated as

$$Z_{in}^{i} = -\frac{E(i)}{I_o}\frac{\tilde{s}_i\rho_b^i}{\alpha_i h_i}\ln\left(\frac{\rho_b}{\rho_a}\right)\left[\left(\phi_s-\tilde{\phi}_i\right)\left(z_s-\tilde{z}_i\right)\right] \tag{11}$$

which must be summed over the four radial edges of the element which contains the feed. Having specified the FE-BI system, interior excitation functional and appropriate antenna parameters such as gain and input impedance, the formulation may be used to analyze the radiation characteristics of several interesting configurations.

3 Results

The FE-BI formulation presented in [8] may be used for antenna performance studies by making the modifications outlined in this paper. This method can be used to determine the role of curvature in the radiation pattern and the input impedance of a cavity-backed patch antenna. Additionally, designers are concerned with the effect of the cavity size might have on antenna performance. In particular, since the cavity is used to suppress parasitic substrate

modes, varying the cavity size can be used to determine the effect of such modes on the radiation pattern.

Two types of antenna elements are investigated and they are shown in figure 2 where each patch is $a\alpha^o \times b$ in size with a denoting the radius of the cylinder. A patch whose radiating side walls are axially oriented is termed an axially polarized patch and is fed at $\phi_s = \frac{\alpha}{2}$. Circumferentially (or azimuthally) polarized patches have radiating walls forming constant z-surfaces and are typically fed at $z_s = \frac{b}{2}$. Observation in the $\theta = 90^o$ plane is the E-plane for circumferentially polarized patched and the H-plane for axially polarized elements. The terminology originates with the cavity model for patch antennas. We will now characterize a typical cavity-backed patch antenna.

Several computed and measured antenna patterns have been published for patches printed on a coated cylinder. One such patch, which is 3.5 cm × 3.5 cm, was used by Sohtell [11] to compare the accuracy of the cavity model [4] to a surface current integral equation [5]. The measured data was taken at 2.615 GHz for a metallic cylinder which was 63.5 cm long and had a radius of a = 14.95 cm. The cylinder was coated with a 0.3175 cm uniform dielectric having relative permittivity of $\epsilon_r = 2.32$. Data was taken for $-180^o \leq \phi \leq 180^o$ in the $\theta = 90^o$ plane corresponding to the E-plane for circumferentially polarized elements and the H-plane for axially polarized ones. Figure 3 compares these measured patterns with data generated using the FE-BI formulation for an identical patch placed within a $360^o \times 7$ cm cavity. This wraparound cavity best simulated the measured coated cavity. Note that the H-plane patterns are symmetric due to the symmetric placement of the feed, whereas the E-plane patterns are not symmetric. The placement of the feed was not specified in [11]; however, the agreement for the E-plane pattern shown in figure 3 indicates that the position used in the FE-BI model ($a\phi_s$ = -1 cm) is reasonable. The feed was placed at z_s = -1 cm for the axially polarized (H-plane) case.

In a previous paper [8], discrete cavity arrays were found to have a significantly lower radar cross section (RCS) compared to a wraparound array. Thus, the size of the cavity had a significant effect on the scattering properties of the array. The two antennas presented by Sohtell [11] were placed within cavities which were 7 cm high and approximately 30, 50, 90, 180, 270 or 360 degrees in angular extent. Figure 4 illustrates that azimuthal cavity size has little effect on the radiation pattern for a circumferentially polarized element. A similar comparison for the axially polarized patch is shown in

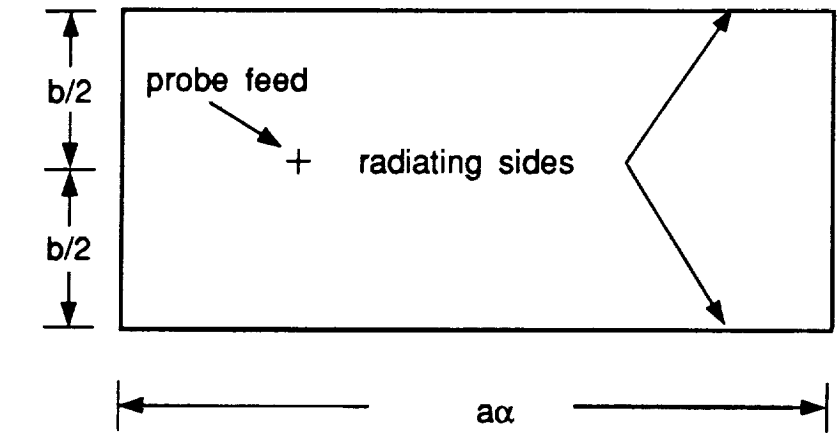

(a)

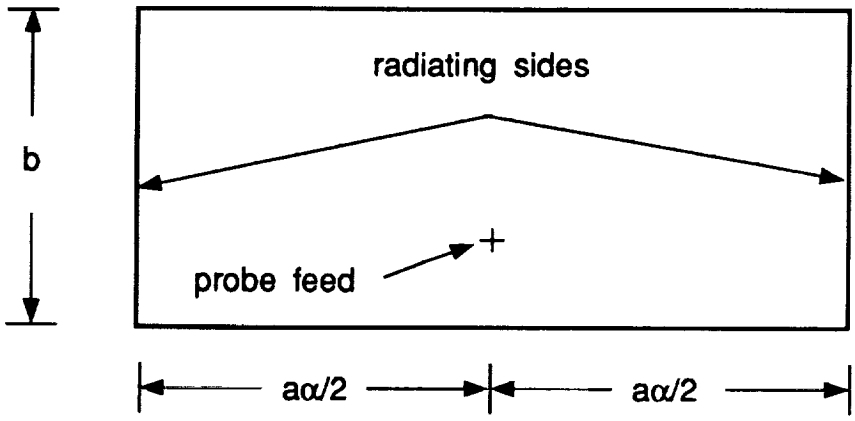

(b)

Figure 2: Illustration of (a) a circumferentially polarized patch element; and (b) an axially polarized patch element. The radius of the cylinder is denoted by a.

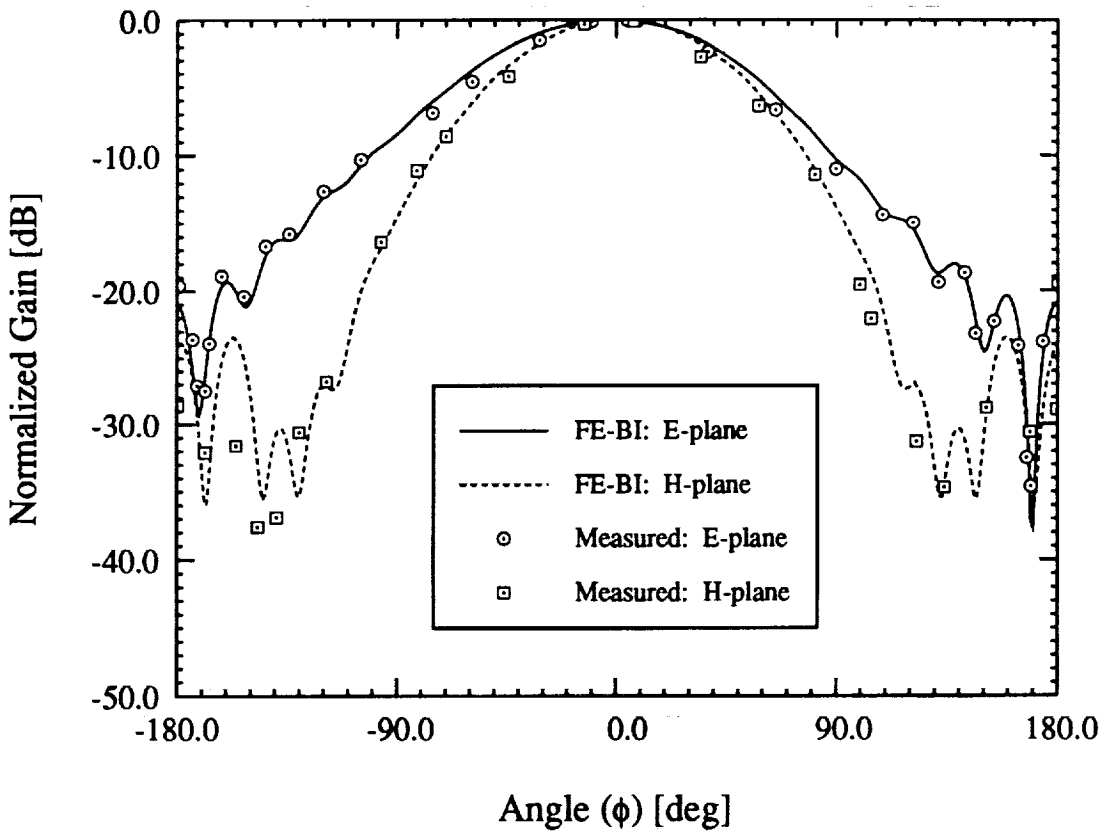

Figure 3: Comparison of measured [11] and computed data for a circumferentially polarized element (E-plane) and an axially polarized element (H-plane). The antenna (3.5 cm $\times$ 3.5 cm) was printed on a 14.95 cm cylinder with a 0.3175 cm coating ($\epsilon_r = 2.32$). The probe feed was place at $(a\phi_s, z_s)$ = (-1.0,0.0) for the circumferentially polarized patch and at $(a\phi_s, z_s)$ = (0.0,-1.0) for the axially polarized antenna.

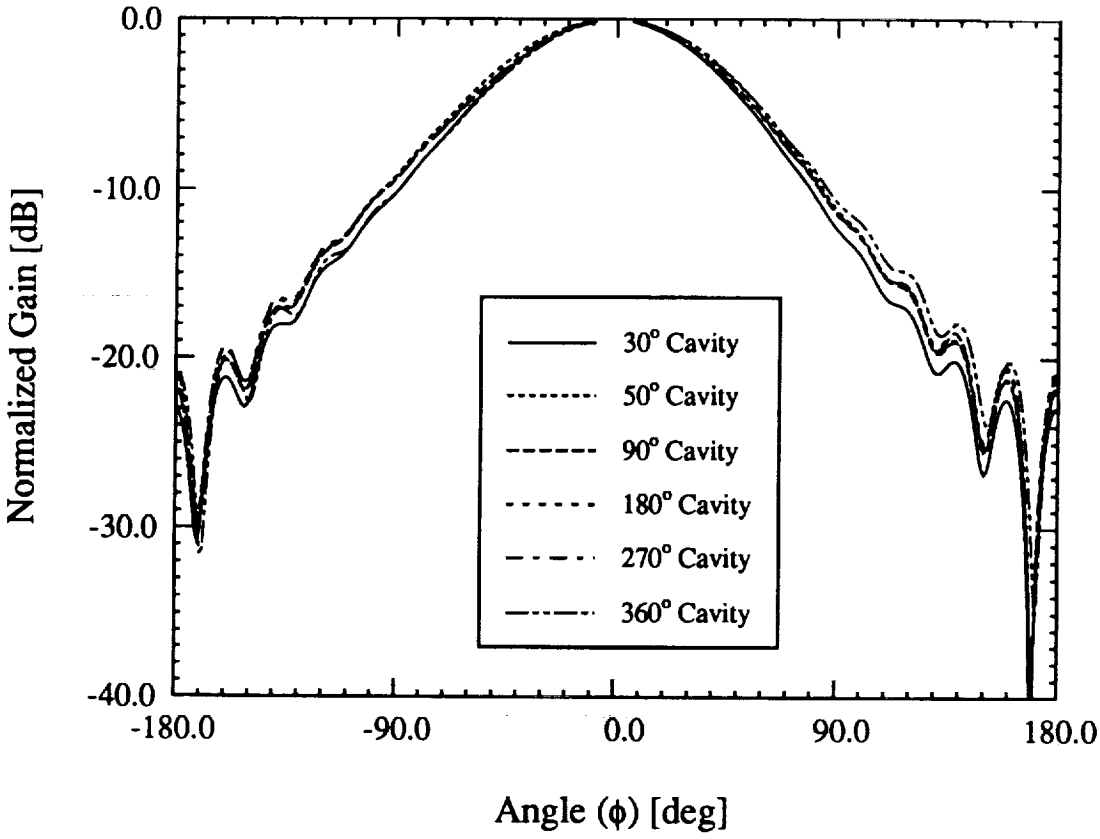

Figure 4: Effect of cavity size on the E-plane radiation pattern of a circumferentially polarized patch antenna.

figure 5. The back lobe of the antenna (near $\phi = 180^0$) is very small for cavities less than 180° in extent but increases for larger cavities. For cavities which lie on the forward face of the cylinder, the substrate modes diffract off the cavity walls; an effect which has little influence on the main lobe of the pattern. However, for wraparound cavities and cavities which extend into the back side of the cylinder, the substrate modes shed like creeping waves giving rise to the back lobe.

Having established the effect of cavity size on the antenna patterns, it is instructive to gauge the effect that curvature has on the resonance behavior (or gain) of patch antennas. The two antennas were placed in 14 cm × 14 cm cavities which were place on cylinders with increasing radius. The frequency was allowed to vary from 2.4 GHz to 2.7 GHz and the peak radiated power was recorded at each frequency. For this paper, the radiated power is recognized as the first term of (8). Figure 6 illustrates that the resonance frequency increases with increasing curvature for a circumferentially polarized antenna, but the maximum gain is similar regardless of element curvature. Note in the cavity model, the radiating edges for a circumferentially polarized patch are the azimuthal walls of the cavity (see figure 2) which have a constant separation regardless of the cylinder radius. However, the axially polarized patch has decreasing resonant gain with increasing curvature as shown in figure 7. For this patch, radiation is attributed to the axial magnetic walls of the cavity model which have increasing angular separation with decreasing curvature. These walls radiate strongly away from the pattern peak ($\phi = 0°$). Accordingly, the gain of an axially polarized antenna decreases with increasing curvature. The radiation pattern of a circumferentially polarized antenna is largely unaffected by curvature as shown in figure 8 when excited at a resonant frequency. However, the radiation pattern of the axially polarized antenna broadens as the curvature increases and this is illustrated in figure 9. Once again, both relationships are readily explained by considering the effect that curvature has on the orientation of the cavity model radiating walls.

In addition to the gain and pattern of an antenna, designers require the input impedance for matching purposes. For the antenna examined above (in a 14 cm × 14 cm cavity), the input impedance was calculated from 2.4 GHz to 2.7 GHz for various cylinder radii. Figure 10 illustrates that the input impedance of a circumferentially polarized patch antenna is not affected by curvature while figure 11 shows that increased curvature reduces the input

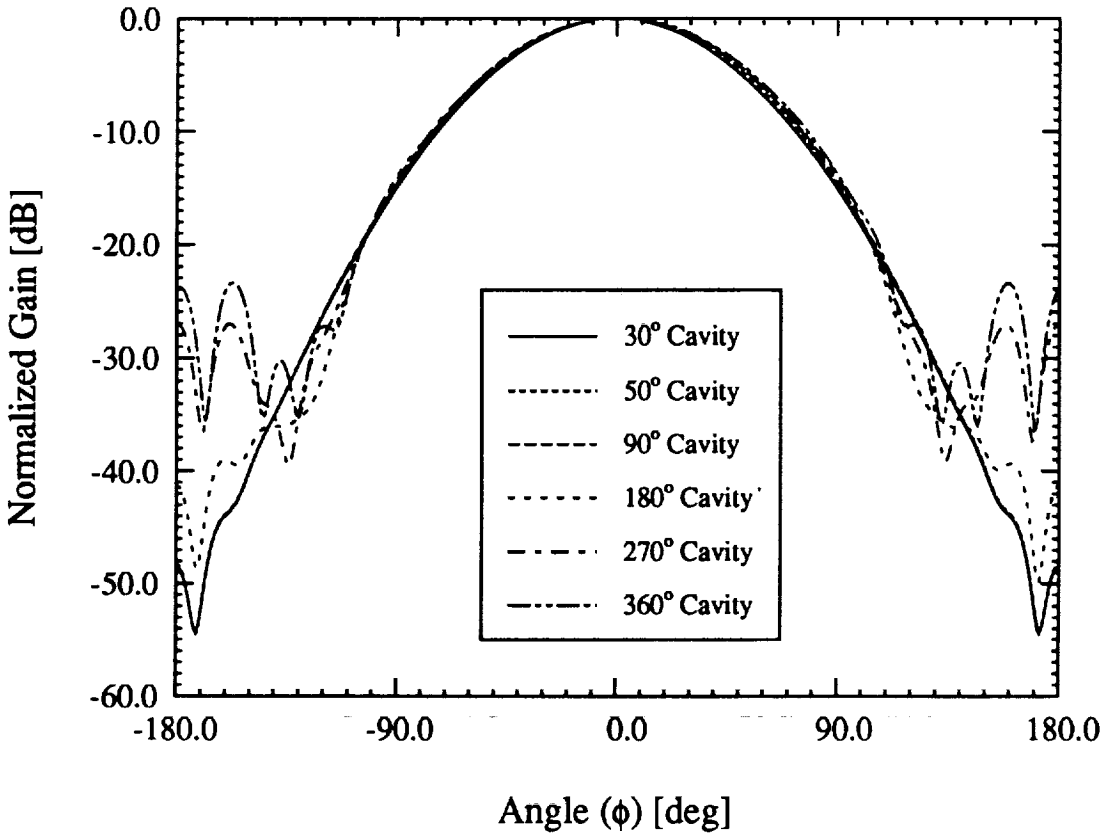

Figure 5: Effect of cavity size on the H-plane radiation pattern of an axially polarized patch antenna.

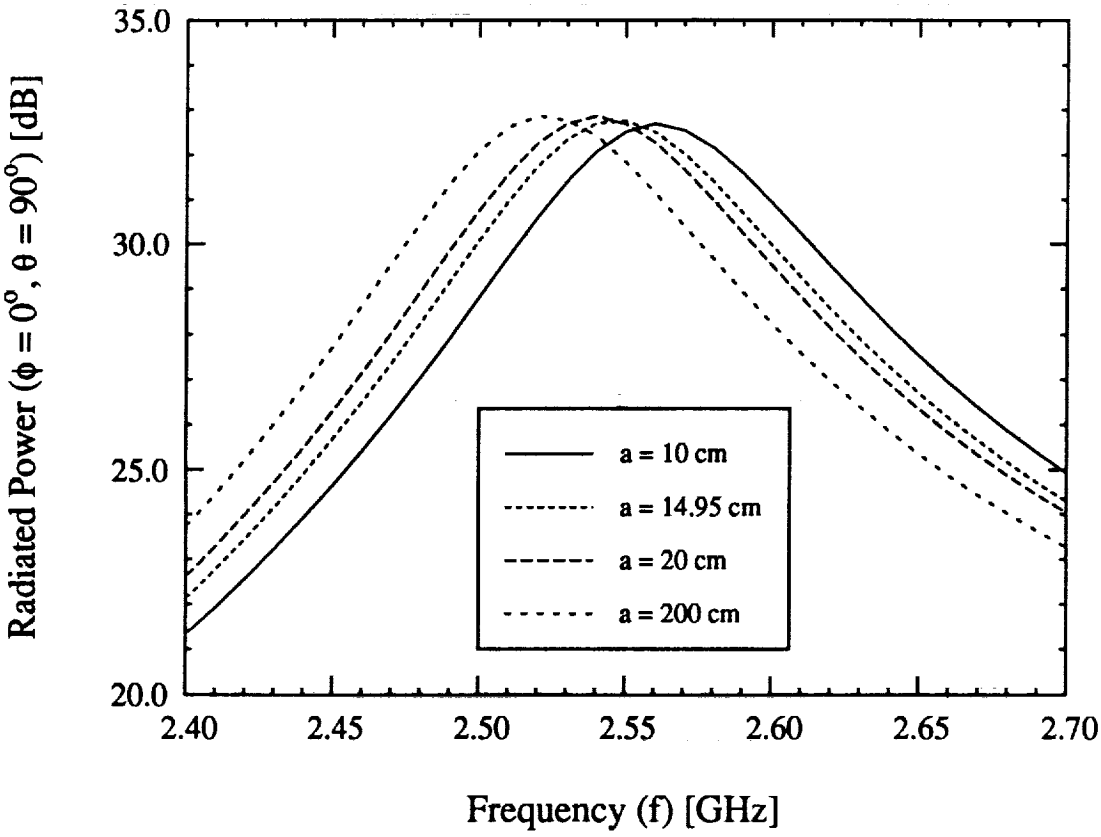

Figure 6: Resonance behavior of a circumferentially polarized patch antenna for various cylinder radii.

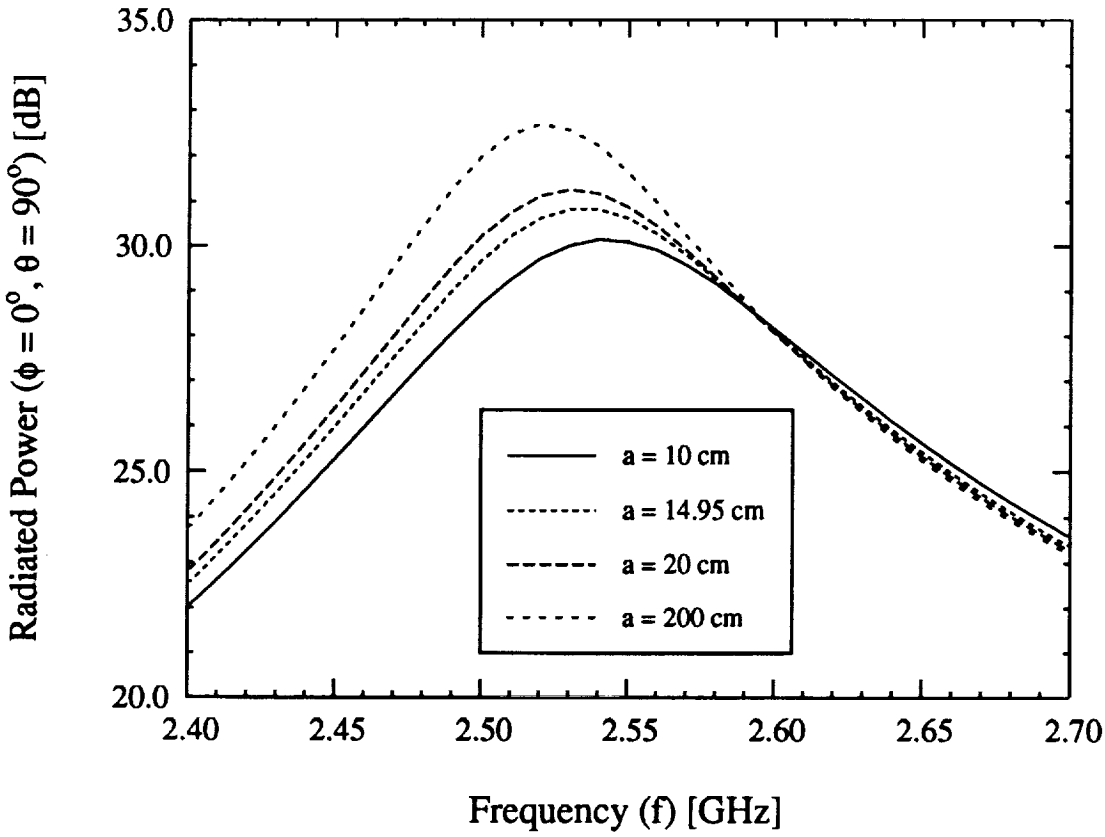

Figure 7: Resonance behavior of an axially polarized patch antenna for various cylinder radii.

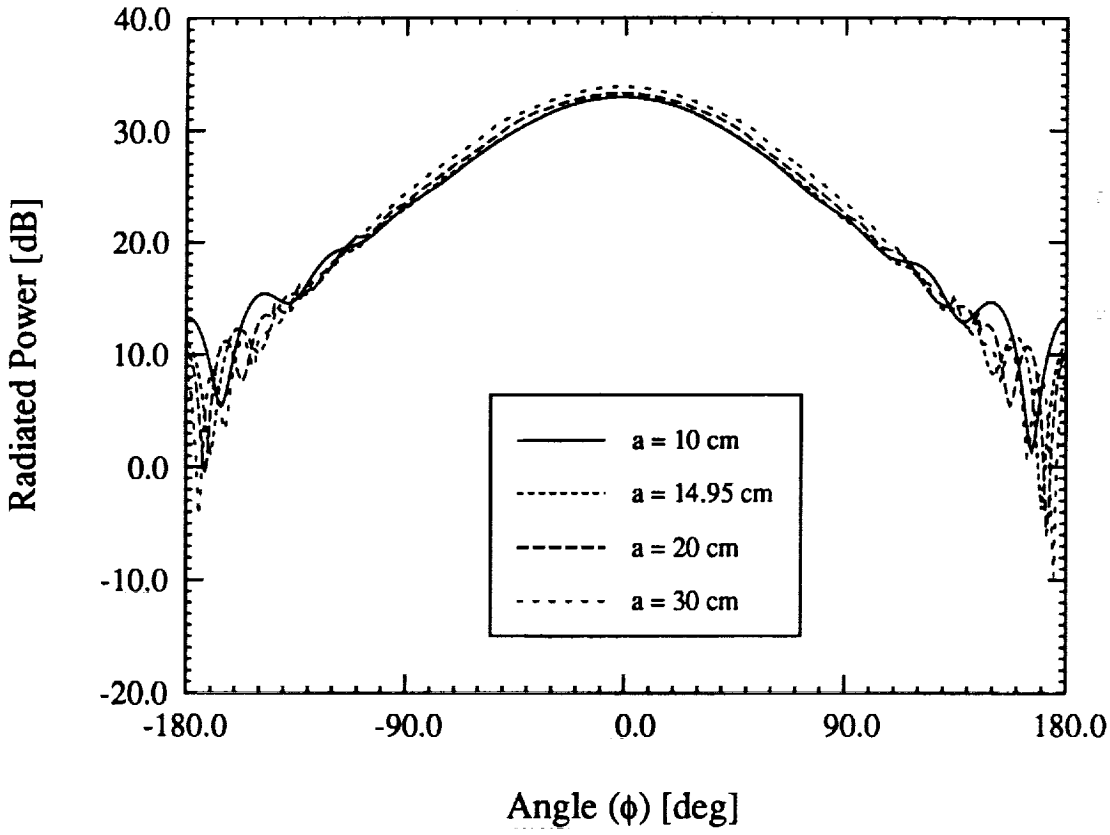

Figure 8: Variation of the radiation pattern shape with respect to curvature for a circumferentially polarized antenna.

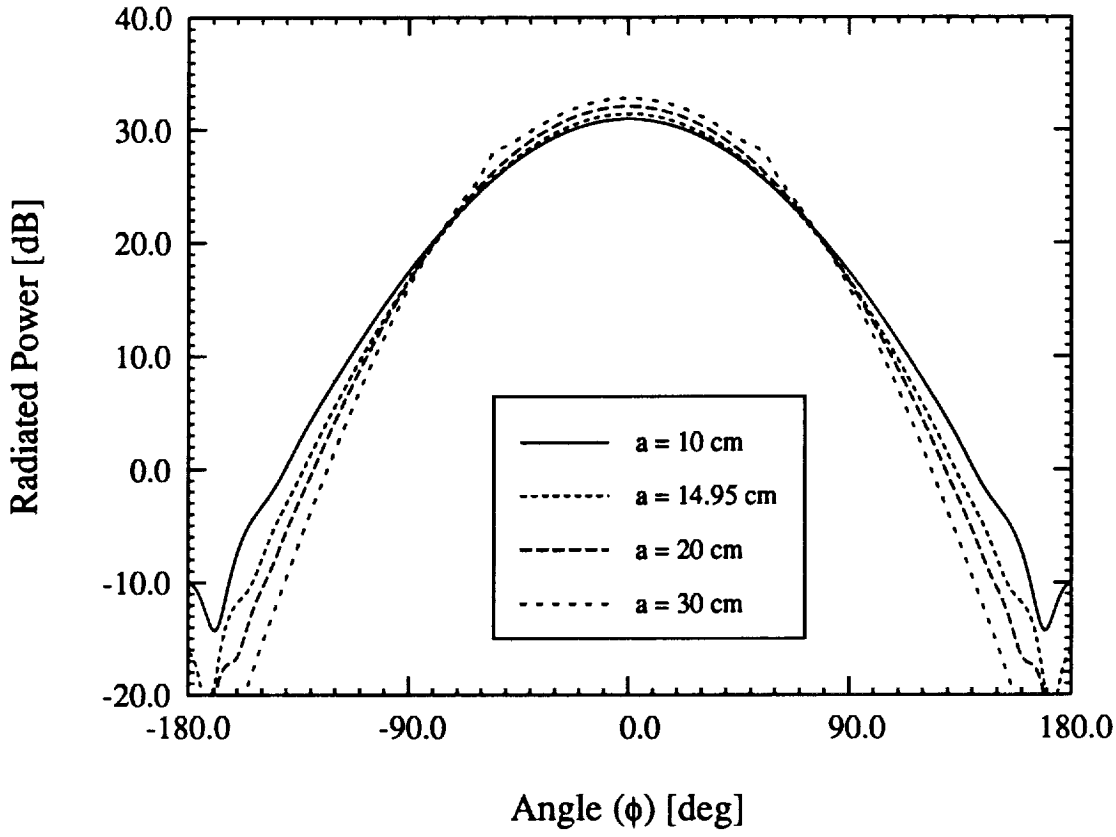

Figure 9: Variation of the radiation pattern shape with respect to curvature for an axially polarized antenna.

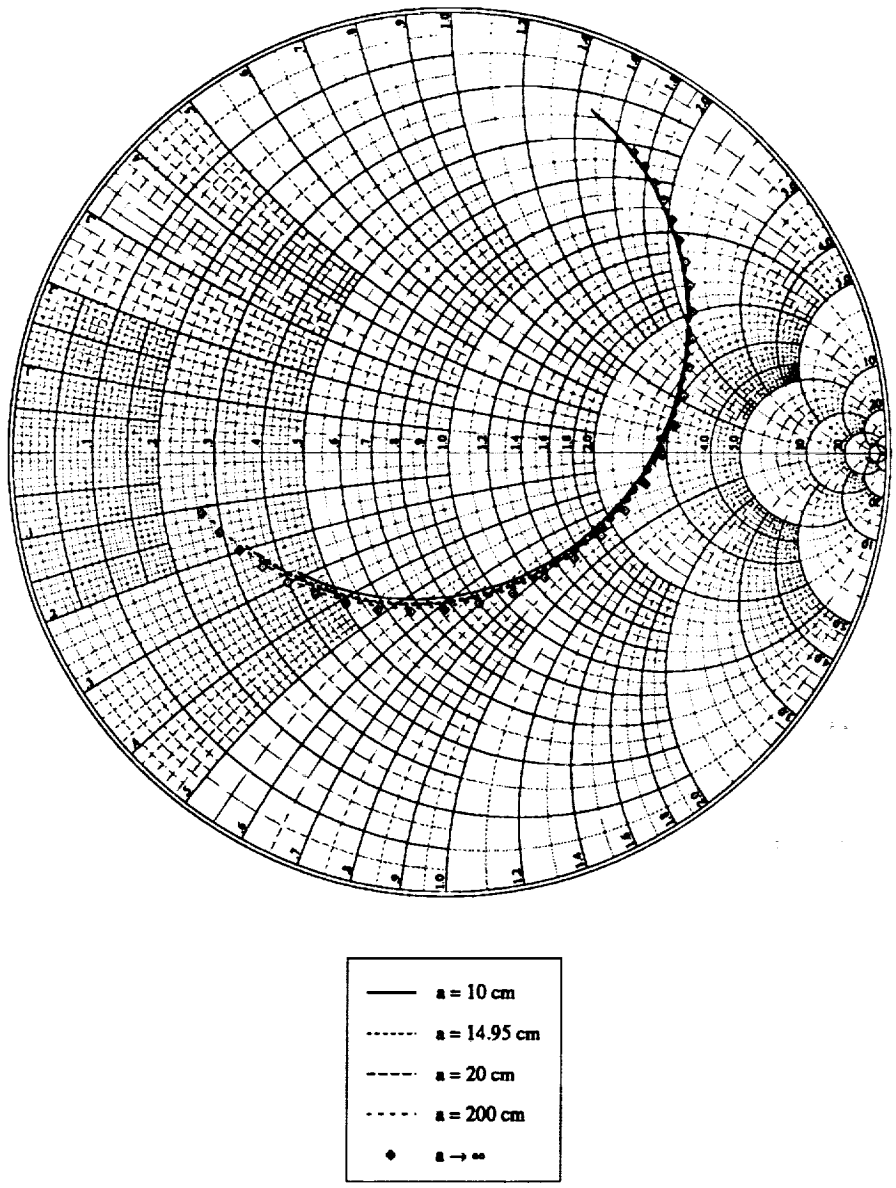

Figure 10: Input impedance of a circumferentially polarized patch antenna for various cylinder radii. The frequency range was 2.4 GHz to 2.7 GHz and the cavity size was 14 cm × 14 cm.

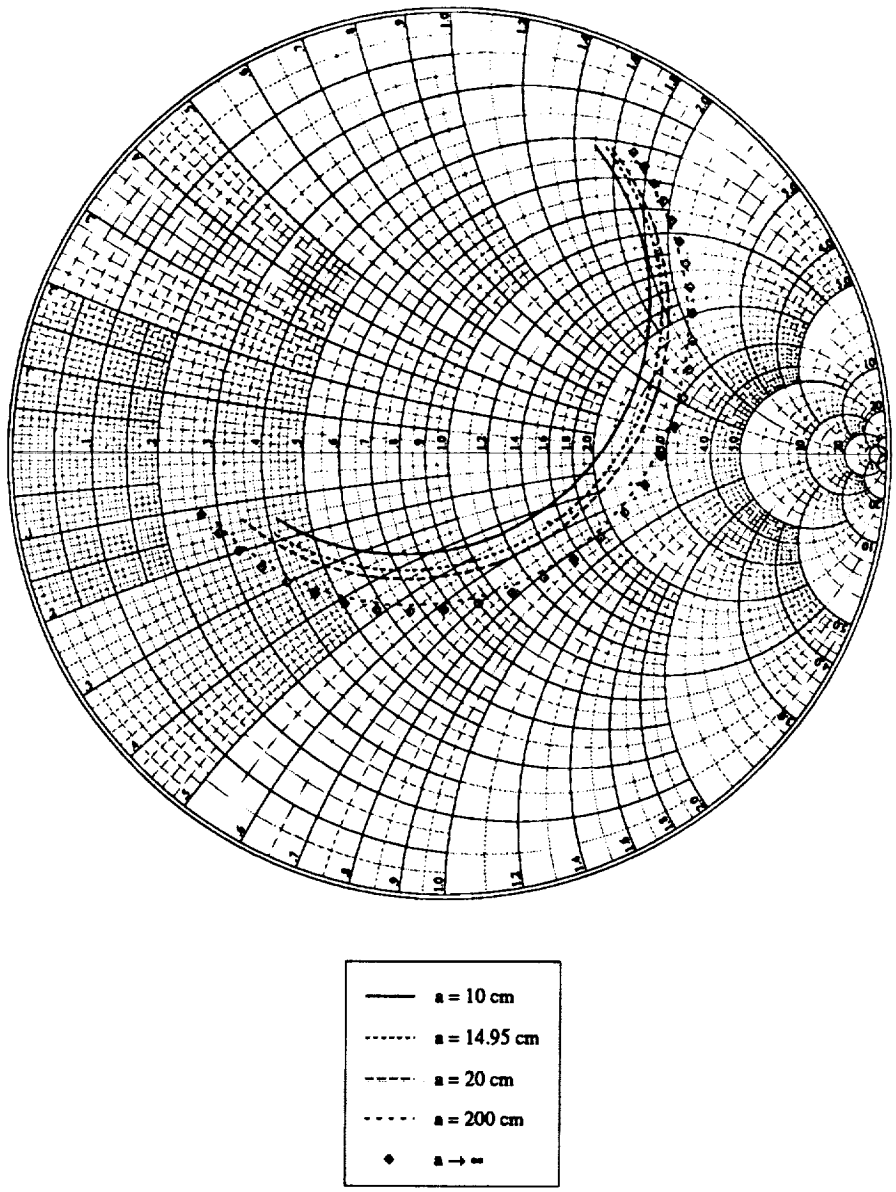

Figure 11: Input impedance of an axially polarized patch antenna for various cylinder radii. The frequency range was 2.4 GHz to 2.7 GHz and the cavity size was 14 cm $\times$ 14 cm.

impedance of an axially polarized patch. This observation agrees the the results reported by Luk *et. al.* [12].

In addition to single patches, the FE-BI formulation may be used to design microstrip arrays. Such an approach includes mutual coupling between elements which is ignored by the cavity model. Furthermore, the FE-BI formulation consumes less computational resources than a comparable integral equation formulation due to the sparsity of the FE matrix. The H-plane pattern of a four element array was measured to gauge the accuracy of the FE-BI approach. Each element is 2 cm $\times$ 3 cm and placed within a 5 cm $\times$ 6 cm $\times$ 0.07874 cm cavity which is filled with a dielectric having $\epsilon_r = 2.17$. The cylinder is 91.44 cm long and has a radius of 15.24 cm. The cavities are placed symmetrically around the cylinder (e.g. a patch is centered at 0^o, 90^o, 180^o and 270^o). Only the patch centered at 0^o was excited while the remaining patches were terminated with a 50Ω load. The driving patch is axially polarized and the feed is located at $z_s = -0.375$ cm. Figure 12 illustrates the excellent agreement between the FE-BI formulation and the measured data.

4 Conclusions

In this paper, the FE-BI formulation for cavity-backed antennas was presented. The data generated by this code for a common cylindrical-rectangular patch antenna compared favorably with measured data. Having validated the implementation, the FE-BI method was used to study the radiation properties of a circumferentially and axially polarized patch antenna. The azimuthal cavity size was found to have little effect on the circumferentially polarized E-plane pattern. However, for the H-plane pattern of an axially polarized element, the back lobe is significantly larger for cavities which extend from the front side to the back side of the cylinder. A wraparound antenna exhibited the largest back lobe implying that this lobe is a result of creeping wave shedding. Diffraction due to the creeping wave is suppressed for cavities not extending to the back side of the cylinder. The presence of a back lobe must be considered when designing low observable, jam-resistant antennas or antennas on complex platforms (e.g. an antenna near the rear stabilizer). Thus, as was the case for scattering reduction, it is advisable to use the smallest cavity possible.

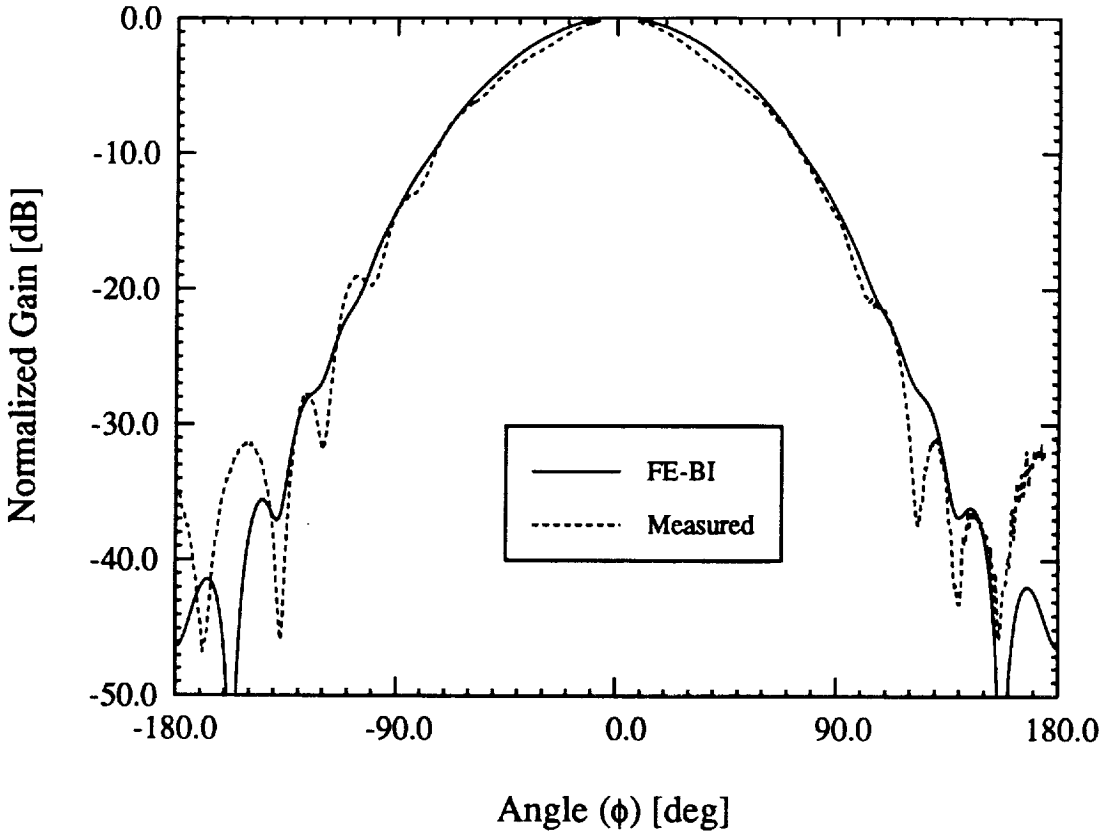

Figure 12: H-plane pattern for a four element patch array. Each patch is 2 cm $\times$ 3 cm and are placed symmetrically around the cylinder. Only the patch centered at 0° is fed while the other patches are terminated with 50Ω loads.

The effect of curvature on the resonance, radiation pattern shape and input impedance was studied. Both circumferentially and axially polarized antennas were considered and was found that the resonant frequency increased with increasing curvature for both antennas. However, while the gain of the circumferentially polarized patch remained constant, the gain of the axially polarized patch decreased with increasing curvature. Such an effect is readily explained by considering which walls of the cavity model radiate for each polarization (see figure 2). The radiation pattern for axially polarized antennas broadens with increasing curvature while the corresponding patterns for circumferentially polarized antennas is unaffected by curvature. The input impedance of the circumferentially polarized antenna was not affected by curvature while the input impedance of the axially polarized antenna decreased with increasing curvature. We therefore conclude that axially polarized antennas are strongly affected by curvature while circumferentially polarized antennas are not affected by curvature.

Since the cavity model does not include mutual coupling and the usual integral equation formulations are associated with high storage and computational demand, the FE-BI formulation is attractive for array analysis. The H-plane pattern of a discrete four element wraparound array compared favorably with measured data.

References

[1] Y.T. Lo, D. Solomon and W.F. Richards, "Theory and experiments on microstrip antennas," *IEEE Trans. Antennas and Propagat.*, Vol. 27, pp. 137-145, 1979.

[2] D.M. Pozar and S.M. Voda, "A rigorous analysis of a microstripline fed patch antenna," *IEEE Antennas Propagat.*, Vol. 35, pp. 1343-1350, Dec. 1987.

[3] J.R. James and G.J. Wilson, "Microstrip antennas and arrays, Pt. 1 – Fundamental action and limitations," *IEE J. Microwaves, Optics, and Acoustics*, Vol. 1, pp. 165-174, 1977.

[4] J.S. Dahele, R.J. Mitchell, K.M. Luk and K.F. Lee, "Effect of curvature on characteristics of rectangular patch antenna," *Electronics Letters*, Vol 23, pp. 748-749, 2 July 1987.

[5] J. Ashkenazy, S. Shtrikman and D. Treves, "Electric surface current model for the analysis of microstrip antennas on cylindrical bodies," *IEEE Antennas Propagat.*, Vol. 33, pp. 295-300, Mar. 1985.

[6] J. Aberle, "On the use of metallized cavities backing microstrip antennas", *1991 IEEE Antennas and Propagat. Soc. Int. Symp.*, Vol. 1, pp.60-63, June 1991.

[7] J-M Jin and J.L. Volakis, "A hybrid finite element method for scattering and radiation by microstrip patch antennas and arrays residing in a cavity," *IEEE Trans. Antennas and Propagat.*, Vol. 39, No. 11, pp. 1598-1604, Nov. 1991.

[8] L.C. Kempel and J.L. Volakis, "Scattering by cavity-backed antennas on a circular cylinder," submitted to *IEEE Trans. Antennas and Propagat.*.

[9] J.L. Volakis, A. Chatterjee and J. Gong, "A class of hybrid finite element methods for electromagnetics: A review," to appear in *J. Electromagnetic Waves Appl.*, 1994.

[10] T.M. Hashaby, S.M. Ali and J.A. Kong, "Input impedance and radiation pattern of cylindrical-rectangular and wraparound microstrip antennas,"

IEEE Trans. Antennas and Propagat., Vol. 38, No. 5, pp. 722-731, May 1990.

[11] E.V. Sohtell, "Microstrip antennas on a cylindrical surface," in *Handbook of microstrip antennas*, Ed. J.R. James and P.S. Hall, Peregrinus: London, pp. 1227-1255, 1989.

[12] K-M Luk, K-F Lee and J.S. Dahele, "Analysis of the cylindrical-rectangular patch antenna," *IEEE Trans. Antennas and Propagat.*, Vol. 37, No. 2, pp. 143-147, Feb. 1989.